



EPTT-2022-0087

PERFORMANCE OF RANS-BASED TURBULENCE MODELS ON A PILOT SCALE, HYDROFOIL IMPELLER DRIVEN, STIRRED TANK.

Eduard Rubens Schacht Sasse¹

erssasse@furb.br

Alessandra Letícia Longhi¹

allonghi@furb.br

Celso Murilo dos Santos¹

celsomurilo@furb.br

Leonardo Lima Magalhães²

leonardo_lmagalhaes@outlook.com

Jonathan Utzig¹

jutzig@furb.br

Henry França Meier¹

meier@furb.br

¹ University of Blumenau, Blumenau – Brazil

² WTech Indústria e Comércio LTDA, Biguaçu – Brazil

Abstract. *The vigorous, swirling flow induced by mechanical mixing stirrers renders them a CFD modelling challenge. Aiming the numerical validation of the single-phase flow in 1 m³ pilot scale square-section tank agitated by a broad blade hydrofoil-type impeller, multiple RANS-based turbulence models are evaluated, – namely, standard k-ε, k-ε Realizable, k-ε RNG, k-ω, SST and RSM. The solution is verified against experimental data for power. A further comparison is made between power derived from rotor torque and energy dissipated in the fluid to assess the cross consistency of the simulation. GCI method is applied to estimate the numerical uncertainty associated with grid coarseness. Velocity and turbulence dissipation rate are also verified on local profiles. Generally, little sensitivity is found on velocities and overall properties among turbulence models. Power can be predicted within 10% of experimental value. Turbulent properties, comparatively, are substantially sensitive to mesh resolution and turbulence model. The presented work is preliminary and lack further numerical and experimental analysis.*

Keywords: *CFD, stirred tank, single-phase flow, turbulence modeling, experimental validation.*

1. INTRODUCTION

Since the introduction of methods for the prediction of impeller motion, computational fluid dynamics has been widely used for simulation of industrial stirred tanks on their many applications. Moreover, recent advances on computational hardware and of modeling methods render possible all-featured solutions of complex multi-dynamic stirred systems, such as biological sludge vessels (Wodołazski, 2020).

Although state-of-art CFD allow for reliable solutions of fully resolved multiphase reacting systems, single-phase simulations remain a relevant and reachable starting point for the validation of the computational model. This can be useful for establishing the fundamental methods for the following, more convoluted, simulations. As of today, approaches based on time-averaged flow governing equations, namely RANS equations, remain the main techniques for solving applied large-scale industrial problems. These rely on turbulence modelling, which depend on empirically obtained parameters. Such dependence renders inexact solutions to the manifold of problems which these are typically applied upon. Therefore, a comparison between model dependent solutions and experimental data is requested for testing the reliability of the former.

Although two-equation, isotropic, turbulence models are computationally inexpensive, their major shortcoming arise from underresolving details of turbulent structures (Menter, 2009), which can lead to poor prediction of turbulent quantities, thus of the power number of an impeller if derived therefrom (Jaworski and Zakrzewska, 2002; Yeoh et al.,

2004; Murthy and Joshi, 2008; Singh et al., 2011). This drawback can be extended to other phenomena dependent on said quantities, such as mass and heat transfer, crystallization and bubble break-up, all of which are commonly found in mixing operations.

Jaworski and Zakrzewska (2002) compared several RANS-based models for the prediction of the wall-jet induced by a PBT impeller in a baffled stirred tank. These simulations were compared to LDA results. It was found that axial and tangential velocities are predicted within 6% or less of the experimental value whereas turbulent kinetic energy is severely underpredicted, even by the anisotropic RSM model. For the Rushton turbine Yeoh et al. (2004) made a comparison between the standard RANS- $k-\varepsilon$ and LES-Smagorinsky models. Whereas both approaches are well-suited for the prediction of velocities in the impeller discharge, – in some cases RANS simulations had better agreement with experimental data than its counterpart –, k and ε are underpredicted as much as 50% in the former. Also, the power number can be integrated from the global energy dissipation rate within 15% of the measured value in case of LES. Further evaluating the accuracy of RANS modeling compared to LES, Murthy and Joshi (2008) tested impeller models with different flow characteristics. It was found that standard $k-\varepsilon$ becomes more fitting regarding turbulent quantities as the flow generated by the impeller becomes more convective, in opposition to dissipative. This implies that the two-equation closure tend to be adequate for the simulation of low power number, axial flow, impellers. For instance, in case of a high-efficiency, low power, narrow-blade hydrofoil the predicted power number (experimentally 0.27) is about the same for both models (0.25 and 0.26, respectively). Singh et al. (2011), found the SST model to provide the best compromise between experimental data fittingness and computational cost, even outperforming models such as SAS-SST, – which retains some LES characteristics, – regarding the kinetic turbulence energy prediction in the Rushton turbine discharge region. Comparing multiple finer meshes, up to 21.5 million nodes, Lane (2017) observed a significant dependance of k and ε values with element size in a tank stirred by a Lightnin A-310 impeller. Additionally, it was found that, although $k-\varepsilon$ model underpredicts comparatively less the global dissipation rate throughout the vessel, SST model solves it better at the impeller vicinity. More recently, Alonzo-Garcia et al. (2019), using RANS approach, compared unstructured cutcell and tetrahedral meshes. While both methods provide good results for the prediction of power number and pumping number based on torque and velocity, respectively, no agreement was found on the former property if obtained from turbulent dissipation on a tetrahedral mesh. Several two-equation closures were also compared, deeming the $k-\varepsilon$ realizable as the most appropriate for the prediction of all experimentally validated properties. It is common agreement that isotropic turbulence modelling may be poor for the prediction of turbulent properties although sufficient for representation of the overall flow in stirred tanks. Also, there is a great dependence of said properties with mesh size.

Following the overall methodology applied in previous studies, the current work is aimed towards the validation of a computational model for the flow induced by a broad-blade hydrofoil-type impeller. It is preliminary work for the investigation of gas dispersion systems. In addition, its findings should serve as a guideline for shape-wise, CFD-based, mathematical optimization. Given the latter goal, the main criteria is achieving an inexpensive and numerically-robust, but sufficiently accurate model for predicting overall quantities of the system, mainly power and pumping capacity. As geometry will be systemically varied, unstructured meshes are preferred over structured ones. Stable and cheap, but rather inaccurate low-order methods are also favored over higher order equivalents. More fundamentally, the RANS approach over expensive LES, DES or DNS simulations is a must, hence a range of turbulence closures are put to comparison.

2. EXPERIMENTAL AND NUMERICAL METHODOLOGY

2.1 CFD modeling

In the current work, modeling of the fluid dynamics in the stirred tank has been carried on by the eulerian RANS approach. The time-averaged continuum and momentum governing equations for the incompressible single-phase flow are expressed in Eqs. (1) and (2), respectively.

$$\nabla \cdot \bar{v} = 0 \quad (1)$$

$$\rho \left(\frac{\partial \bar{v}}{\partial t} + \bar{v} \nabla \bar{v} \right) = -\nabla p + \mu \nabla^2 \bar{v} + \rho \cdot g - \rho \frac{\partial \tau_{ij}}{\partial x_j}. \quad (2)$$

Here, \bar{v} stands for the mean velocity, ρ for density, p for pressure, μ for the dynamic viscosity, g is the gravitational acceleration, and τ_{ij} the Reynolds stresses.

Two-equation, isotropic turbulence models rely on the transport of the turbulence kinetic energy (k) and its dissipation rate (ε) for the closure of Reynolds-stress term arisen from the fundamental equations averaging. A general form of the transport equations for these respective properties on incompressible flow can be written as in Eq. (3) and Eq. (4).

$$\rho \left[\frac{\partial k}{\partial t} + \nabla \cdot (k \bar{v}) \right] = \nabla \cdot [(\mu + \mu_t(k, \varepsilon)) \nabla \cdot k] + S_k(k, \varepsilon), \quad (3)$$

$$\rho \left[\frac{\partial \varepsilon}{\partial t} + \nabla \cdot (\varepsilon \vec{v}) \right] = \nabla \cdot [(\mu + \mu_t(k, \varepsilon)) \nabla \cdot \varepsilon] + S_\varepsilon(k, \varepsilon), \quad (4)$$

where μ_t stands for the eddy viscosity and S_k, S_ε are source terms congregates for k and ε , respectively.

A more representative RANS modeling can be archived through second-order closure, as with Reynolds-stress models (RSM), where an equation is solved for each component of the symmetric Reynolds stresses. For non-compressible flow the transport equation can be written as

$$\frac{\partial \tau_{ij}}{\partial t} + \nabla \cdot (\vec{v} \tau_{ij}) = P_{ij} + \Pi_{ij} - \varepsilon_{ij} + D_{ij} + M_{ij}. \quad (5)$$

where P_{ij} is the production term, Π_{ij} is the pressure-strain correlation, ε_{ij} is the dissipation term and D_{ij} is the diffusion.

Simulations were performed on ANSYS FLUENT v19.0. The Sliding Mesh transient method was chosen for the solution of impeller motion. The flow domain is separated between an inner moving zone and an outer static zone. The former rotates in the core of the latter, and solution is proceeded in moving frame of reference. Each time-step increments follows equivalent displacement of the inner rotational zone. On constant rotational speed of moving bodies, structure-to-fluid momentum transfer depends on Coriolis and centrifugal effects. Following the aforementioned criteria of stability and inexpensiveness of solution, momentum and turbulent quantities were discretized by a first order upwind scheme. Convergence criteria for solution residuals was set to 1×10^{-4} for all equations. All solutions were initialized from motionless state and the computation of the time-dependent model was carried until pseudo-stationary condition was reached. Lastly, solution was averaged over time. Reynolds Stress Model (RSM) and several isotropic eddy-viscosity models were compared: standard $k-\varepsilon$, $k-\varepsilon$ RNG, $k-\varepsilon$ Realizable, $k-\omega$ and SST.

2.3 Tank geometry, physical conditions and meshing

The studies were performed in a pilot scale square-section tank with sides length of $T = 1 \text{ m}$ and water height $H = T$. The flow is generated by a broad-blade hydrofoil, Lightnin A-315 alike, impeller. Impeller diameter is equal to $1/5 T = D$ and its clearance to the tank's bottom wall is $3/4 T = C$. All boundaries, except the tank top, are modeled as non-slip condition. The top is set as free-slip condition, emulating air-liquid surface. Impeller is rotated at 100 RPM, characterizing the flow as turbulent at $Re = 6.7 \times 10^4$. The experimental rig is shown on Figure 1. These dimensions and dimension ratios are atypically different to previous published studies on the subject and are purposed towards negligence of wall effects. Such free-flow conditions are commonly found in large-scale sludge treatment tanks.

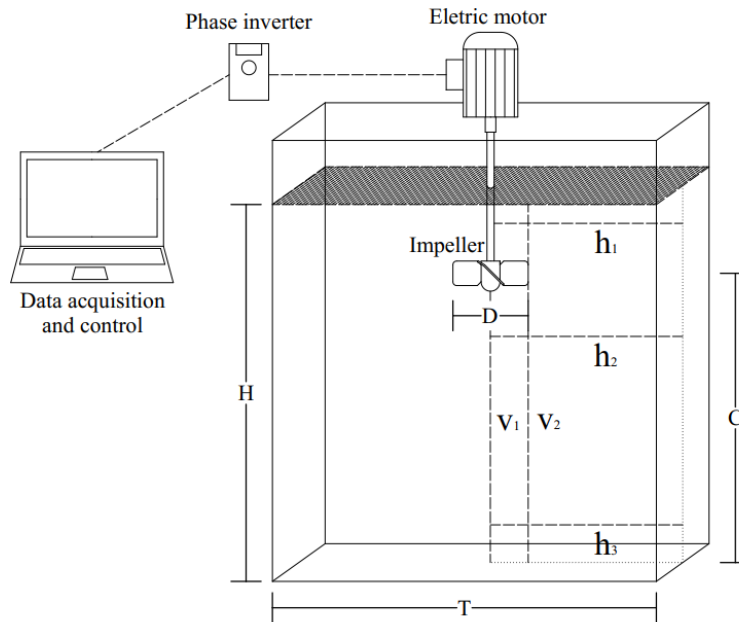


Figure 1. Schematics of experimental rig and plotting line locations.

Pre-processing and post-processing was also done on ANSYS software. The computational geometry of the stirred tank was designed in DESIGNMODELER. The numerical grid was generated on MESHING. The inner and outer zones were meshed independently, rendering non-conformal mesh elements at the interface between them. The irregular-shape inner domain was meshed by non-structured polyhedral elements. The innermost part of static frame zone is composed

by a highly structured hexahedral mesh in a circular pattern while the region close to the side boundaries is meshed as hex dominant prism elements. Following this construction approach of the grid, five different sizes were tested for numerical uncertainty. Length sizes were varied equally among its parameters to assure equivalent ratios along every geometry region. Additional refinement is made nearby impeller. Once computation of the model had been concluded in FLUENT, CFD-POST was employed for data analysis.

Experimentally, stirring power can be estimated based on wire power if inefficiencies are taken account. Although this is an uncommon method and deemed inappropriate by some (Paul et al., 2004) it was successfully used by Hoseini et al. (2021) for characterizing the turbulent power number of a stirrer given the uncertainty of comparison between model and experiment. In the current work, the measure was obtained from estimates on shaft power by a digital Schneider Electric ATV12 phase inverter.

3. RESULTS AND DISCUSSION

3.1 Grid dependence analysis

To evaluate inaccuracy due to mesh coarseness, numerical solutions were tested on five different grid sizes. k-ε Realizable model, considered appropriate for this prior procedure, was used in these simulations. Roache (1994) GCI extrapolation method is applied to estimate the theoretical continuous solution and its uncertainty on overall quantities of the flow.

Three properties are compared along meshes, as is with following model dependent solutions. The measure of the pumping capacity of the impeller is given by flow number (N_q), which can be estimated for axial flow types based on the integration of the normal flux, as given by the axial velocity v_z , over the projected circular surface as

$$N_q = \frac{\int_0^{2\pi} \int_0^{D/2} v_z(r, \theta) dr d\theta}{ND^3}, \quad (5)$$

where N is the impeller rotational speed and D stand for its diameter.

Although normally measured in the discharge region of the impeller, to avoid effects of diverted fluxes, the flow was measured at the height middle section of the impeller. This procedure cannot be easily attained experimentally by usual methods but provide consistent measure regardless of discharge angle on compared CFD solutions.

The most prominent non-dimensional parameter of impellers is the power number, a measure of dissipated power in the stirred vessel. It can be consistently obtained from force distributions over the impeller, hence produced torque on along shaft axis, according to

$$N_{p-\tau} = \frac{\omega \iint_S (\vec{r} \times [n \cdot \sigma(S)]) dS}{\rho N^3 D^5}. \quad (6)$$

Here, ω is the angular velocity of impeller, \vec{r} is a position vector of the cell, n is the normal vector of the cell and σ are the total stresses, given by the sum of pressure and shear stress. An alternative method for the estimation of power number is based on turbulence energy dissipation, as follows:

$$N_{p-\varepsilon} = \frac{\rho \iiint_V \varepsilon(V) dV}{\rho N^3 D^5}. \quad (7)$$

Theory tells all induced power is dissipated, thus $N_{p-\tau}$ should be equal to $N_{p-\varepsilon}$, yet as turbulence is modeled this concept can be severely degenerated on given solution. To assess the discrepancy between these analogous quantities their difference will be quantified. As plain RANS simulations are employed, it is expected for pressure distributions to be more accurate than the solution for turbulent properties, thereby to $N_{p-\tau}$ be more reliable than $N_{p-\varepsilon}$.

Table 1. Grid size dependency and assessed properties on k-ε Realizable model compared to experimental data.

Resolution	N_q	$N_{p-\tau}$	$N_{p-\varepsilon}$	$N_{p-\tau} - N_{p-\varepsilon}$
97,337 elements	0.65	1.91	0.29	1.62
246,110 elements	0.69	1.58	0.35	1.23
489,172 elements	0.71	1.53	0.43	1.10
1,042,382 elements	0.72	1.48	0.50	0.99
2,037,347 elements	0.74	1.47	0.53	0.94
Theoretical continuous	0.78 ± 0.05	1.46 ± 0.01	0.56 ± 0.05	-
Experimental	-	1.60	-	-

Mesh sizes and corresponding quantities are shown on Table 1. All the latter show monotonically converging tendencies and GCI procedure is carried over the solutions of the most refined meshes, providing the estimates for the mesh independent solution on given error band (absolute value on computed GCI_{21}). It can be noticed that N_q and $N_{p-\tau}$ are evaluated with reasonable accuracy even on coarsest of grids. Model prediction of $N_{p-\tau}$ is in reasonable accordance with experimental data, having a deviation of about 10% as to the extrapolated estimative. Also, among all three compared non-dimensional properties, $N_{p-\tau}$ is the least dependent to element size. $N_{p-\varepsilon}$, thus ε , appear to be more sensible to grid size, albeit fairly converged on the most refined one. The difference between $N_{p-\tau}$ and $N_{p-\varepsilon}$ is substantial even on dense meshes and no significant improvement is expected on further refinement, implying faulty modeling. Nonetheless is observed substantial underprediction yet increase of turbulence intensity with mesh refinement.

Spatial variations between solutions will be evaluated along reference profiles on horizontal and vertical axis. Three vertical positions have been chosen for horizontal plots, named h_1 to h_3 . h_1 is located above impeller height, while the other three lines are beneath it. Positions relative to tank bottom are $h_1 = 90$ cm, $h_2 = 35$ cm and $h_3 = 10$ cm. Vertical profiles will be shown on v_1 and v_2 . v_1 is parallel to impeller shaft while v_2 intersects impeller tip radius and crosses the region of most intense flow at discharge. Line locations are shown on Figure 1.

Mixing time is generally related to the largest scales of flow, that is how is the fluid is convected throughout the mixing vessel. Thus, accurate predictions on velocities are paramount for tracking stagnation zones and mixture quality. Pitched blade mixers rely mainly on axial flow to produce this effect. Figure 2 refer to axial velocities on mentioned plotting positions among the five numerical grids. Overall features of the flow can be captured well within all cases except on the sparsest mesh, counting 97K elements, which solves very poorly most regions of the flow, the exception being the upper section of the stirrer tank. For the most part, 246K element mesh characterizes well flow tendencies, although somewhat weakly at lower regions of impeller discharge. Albeit doubling in element number, 489K and 1042K meshes show very similar profiles. Flow reversal point is consistent for all except the coarsest mesh. In general, increase of refinement provide better property magnitude prediction. It can be verified that the most refined, 2 million elements, grid is not ultimately converged on predicted velocity, specially at impeller vicinity and tank's bottom.

Second to macromixing, dependent on liquid flow, turbulence drives mesoscale phenomena, proving mechanism for diffusion and being of uttermost importance for bubble breakup and gas-liquid mass transfer on gas dispersion operations. Turbulence dissipation rate profiles are compared on Figure 3. Note that ε is put on logarithmic scale. Once again, no reliance is found on the coarsest mesh, which deviates one or two orders of magnitude to the remaining curves on most of the cases. The four other profiles lie on the same bias, deviating about two to five time the magnitude value among them. As follows $N_{p-\varepsilon}$ tendency, local turbulence intensities are increased on mesh refinement. The biggest discrepancies are found on impeller discharge. As expected, peak value of this property is found on impeller tip, which is closely predicted among all meshes.

As dominant motion and energy cascade are found on the discharge region, further refinement can be crucial for modelling certain phenomena. Despite all that, quality of prediction for the overall properties, above all $N_{p-\tau}$, which are presented in Table 1, being the main criteria for this study, the intermediary 489K elements mesh was found satisfactory for further analysis of turbulence model dependent solutions.

3.2 Turbulence model dependence

Turbulence models will be compared on the same fashion as to numerical meshes. Axial velocity profiles are shown on Figure 4. Alike solutions are found with standard k- ε , k- ε RNG, k- ε Realizable, k- ω closures. Interestingly, is verified some profile parity on k- ε and k- ε Realizable models as is with k- ε RNG and k- ω . RSM solutions features somewhat deviate from these eddy viscosity models. This is especially noted at impeller discharge plume region, where most energy tends to be dissipated and gradients are steep. Lastly, SST model highly differ from all other model's solutions. In this case, discharge flow is diffused and joined at shaft radius. Opposed to all other solutions, no reverse flux is encountered in this region.

Regarding turbulence energy dissipation (Figure 5), little conformity is observed between models, except for the k- ε and k- ε Realizable pair. Although profiles tendencies are somewhat comparable, magnitude of predicted value range on about one order of magnitude.

Non-dimensional numbers are compared on Figure 6. Following the heterogeneity of turbulence dissipation distributions among models, $N_{p-\varepsilon}$ is somewhat diverse. Standard k- ε and k- ε Realizable share about the same value, at $N_{p-\varepsilon} \cong 0.43$. Although very different ε profiles are found on k- ω , SST and RSM, overall $N_{p-\varepsilon}$ values are close. k- ε RNG underpredicts $N_{p-\varepsilon}$ the most. None of the models seem to provide reliable estimates on N_p based off ε . For all models except SST, $N_{p-\tau}$ is predicted very closely to one another, with values ranging from 1.49 in case of standard k- ε and k- ε RNG to 1.57 for RSM. SST is off at $N_{p-\tau} \cong 2.02$. RSM provide the closest prediction of N_p in respect to experimental data, although some uncertainty can be attributed to grid resolution. N_q variations follow $N_{p-\tau}$ tendencies, where the greatest comparative value is found for SST model, and RSM predicts slightly higher N_q in relation to the remaining four models, all of which characterize this property closely.

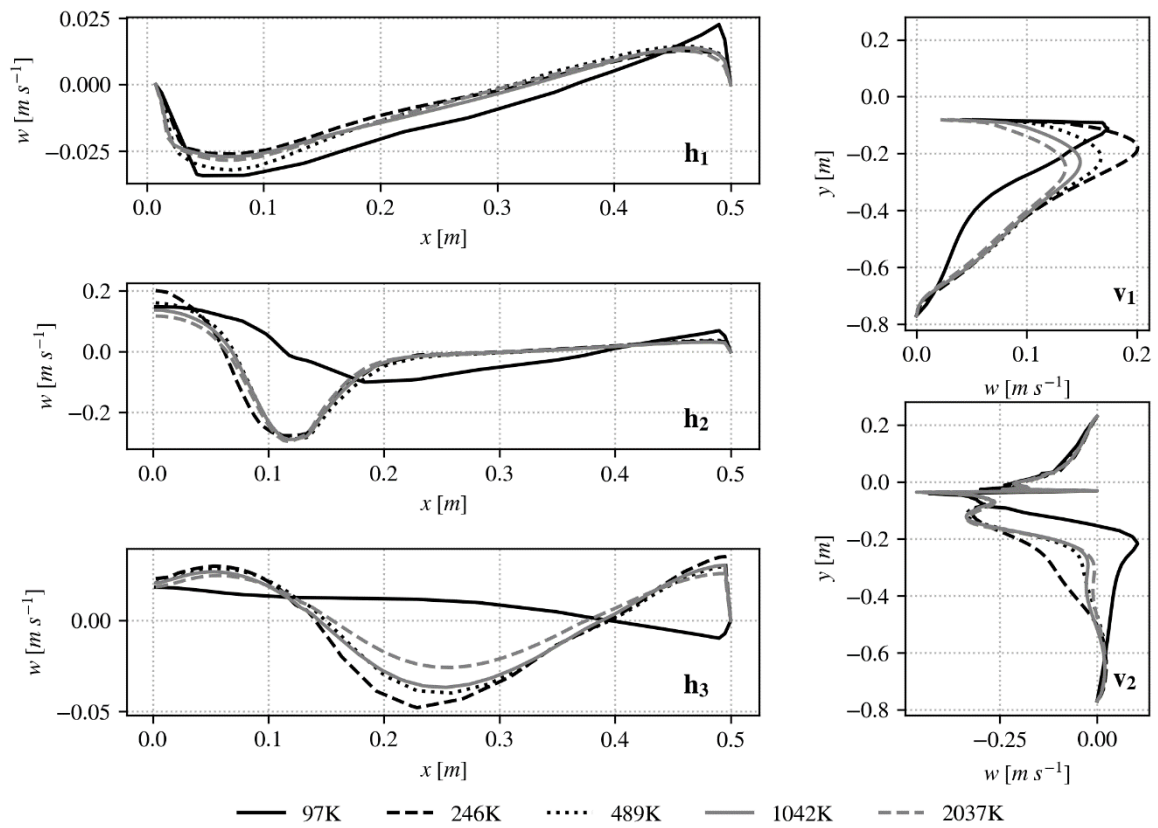


Figure 2. Mesh sensitive comparison of axial velocity (w) profiles.

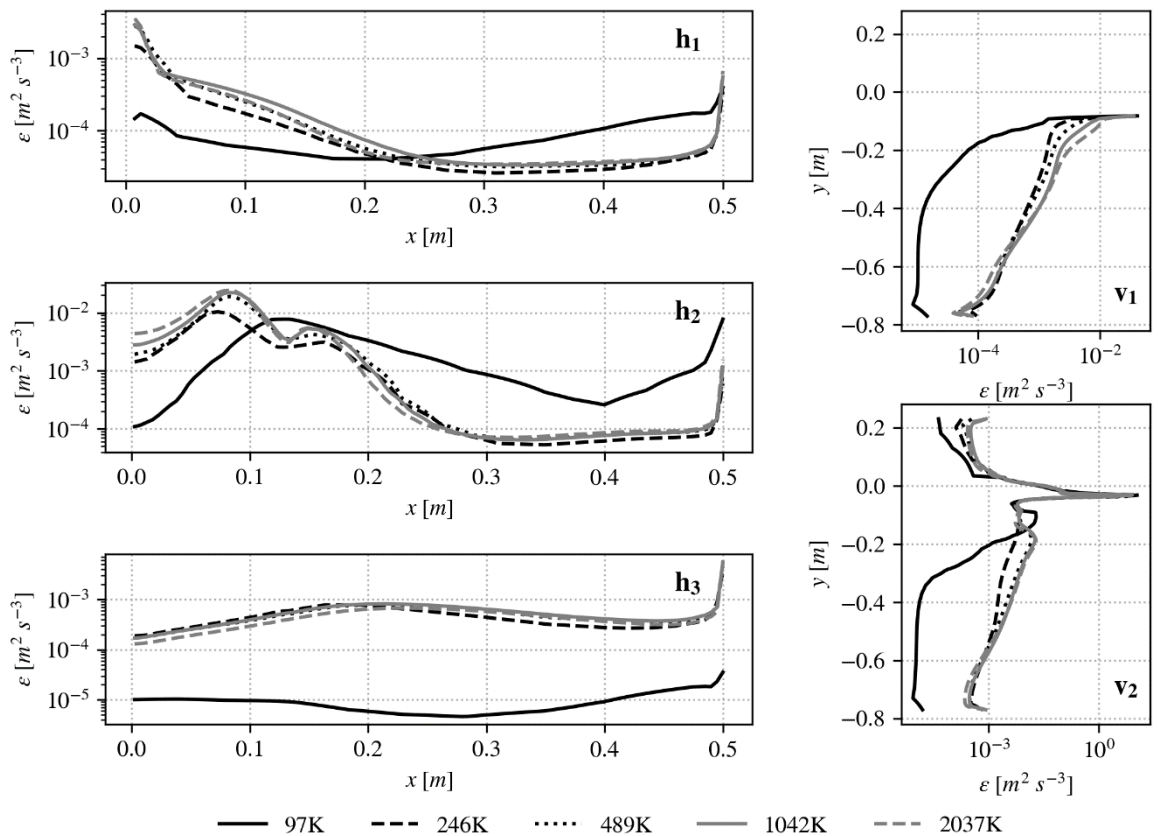


Figure 3. Mesh sensitive comparison of turbulence dissipation rate (ϵ) profiles.

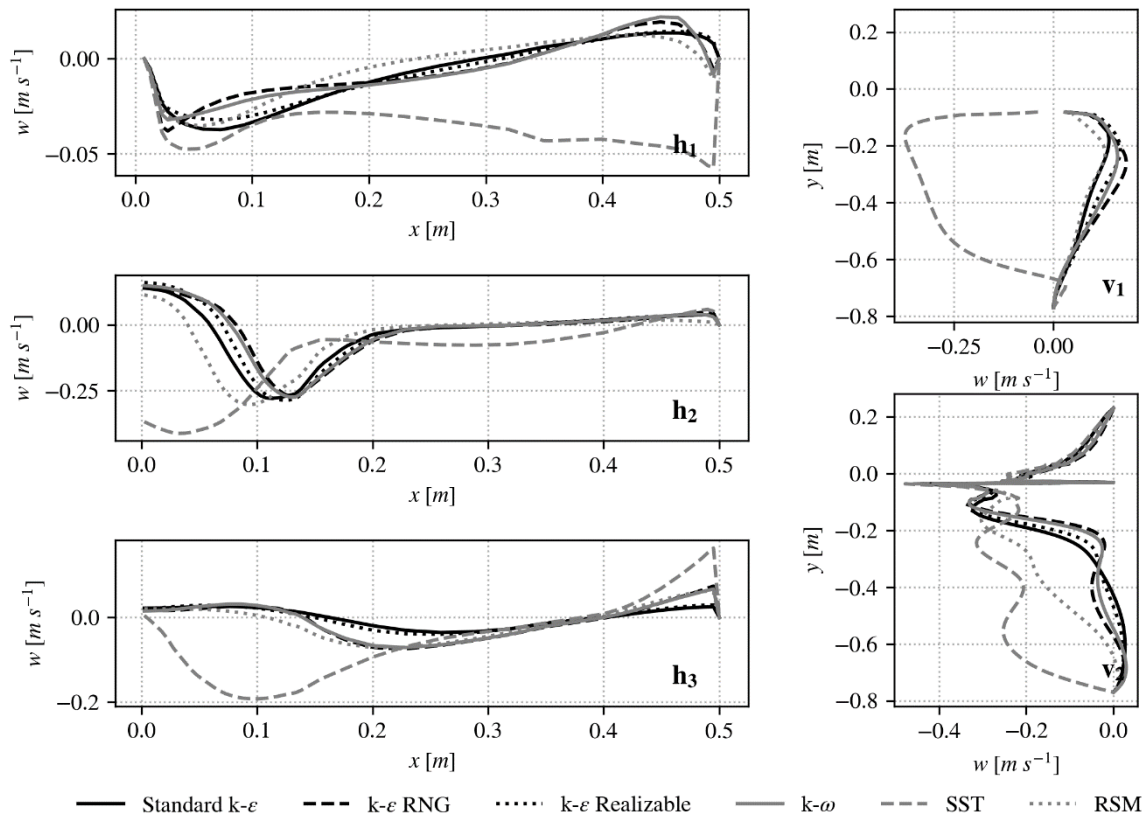


Figure 4. Turbulence model sensitive comparison of axial velocity (w) profiles.

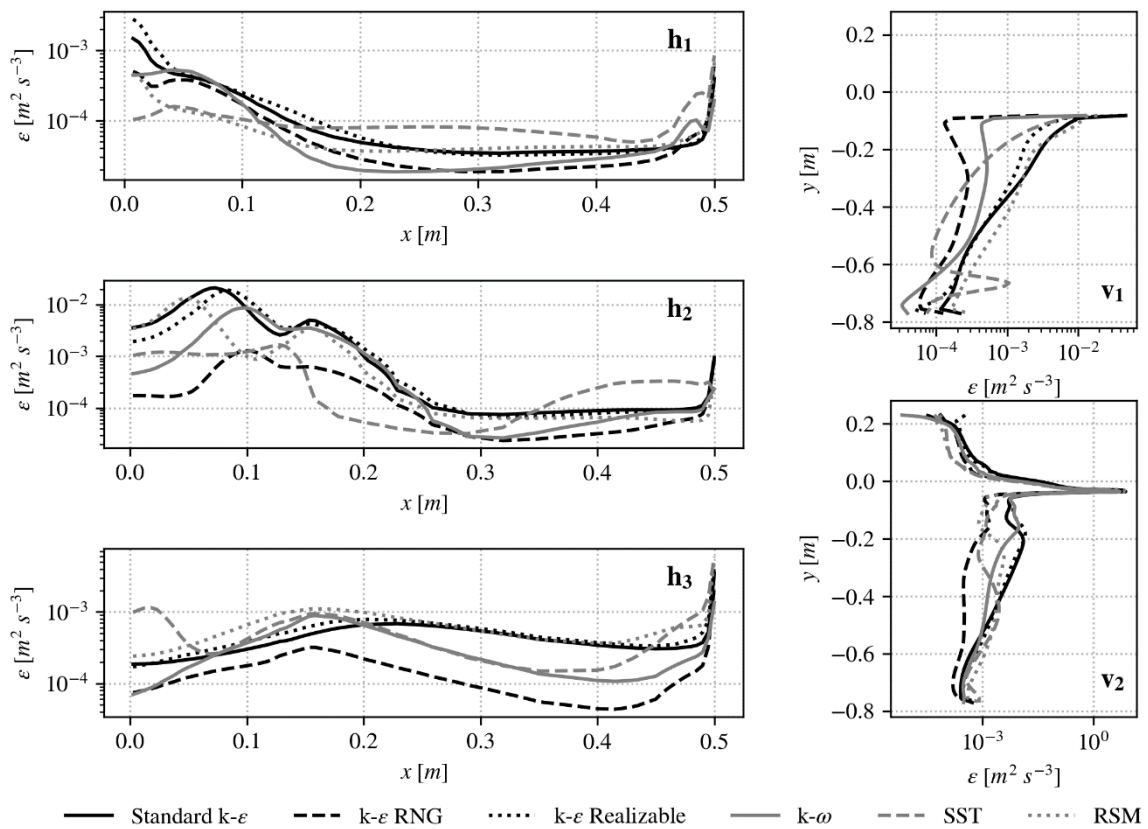


Figure 5. Turbulence model sensitive comparison of turbulence dissipation rate (ϵ) profiles.

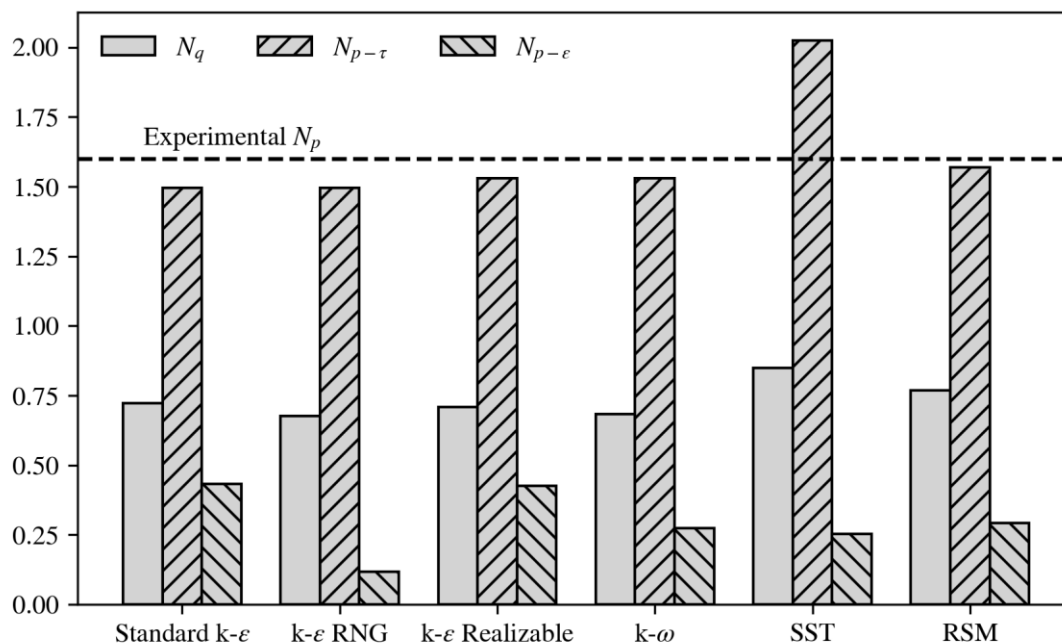


Figure 6. Assessment of turbulence model dependent solution on non-dimensional properties.

Albeit ϵ is crudely quantified, some avail can be found on this degree of predictability. Mass transfer coefficient in gas dispersing systems can be modeled through eddy models, which are based on eddies length on vicinity of the bubbles (Linek et al., 2004). A law is found on $k_L \propto \epsilon^{1/4}$, therefore if, let's say, ϵ is predicted within 30% of the actual value, about 26% deviation is expected from k_L . Such inaccuracy can be tolerated for some purposes.

4. FINAL REMARKS

The presented work is preliminary in the investigation for a robust model for CFD-based optimization of mechanical mixing systems. Several ordinary RANS turbulence models were evaluated on simulation of a pilot scale, square section, stirred tank driven by an axial flow impeller. In general, typical mechanical properties, namely velocity and force, are consistently predicted, generally with little dependence of chosen modeling. No agreement was found on turbulence intensity among models. Alongside, overall turbulence energy dissipation rate seems severely underpredicted for all models. Good agreement was found between numerical and experimental data for power based on induced energy, RSM being the best performant and SST the least. Little endorsement is found for SST model as its solution highly deviate from other model's, expected behavior and experimental data. Nonetheless, given that data for experimental validation is scarce and higher order numerical methods remain uninvestigated, restricted conclusions can be taken on presented results.

5. ACKNOWLEDGEMENTS

The authors are thankful for The National Council for Scientific and Technological Development's (CNPq) and Ministry of Science, Technology, Innovation and Communications. Lastly, WTech Indústria e Comércio is acknowledged for their critical and close collaboration on the current research project.

6. REFERENCES

- Alonzo-Garcia, A., Mendoza-Escamilla, V.X., Martinez-Delgadillo, S.A., Gonzalez-Neria, I., Gutiérrez-Torres, C.d.C. and Jiménez-Bernal, J.A., 2019. "ON THE PERFORMANCE OF DIFFERENT RANS BASED MODELS TO DESCRIBE THE TURBULENT FLOW IN AN AGITATED VESSEL USING NON-STRUCTURED GRIDS AND PIV VALIDATION". Brazilian Journal of Chemical Engineering, Vol. 26, N. 01, p. 361-382.
- Hoseini, S. S., Najafi, G., Ghobadian, B., Akbarzadeh, A. H., 2021. Impeller shape-optimization of stirrer-tank reactor: CFD and fluid structure interaction analyses. Chemical Engineering Journal, V. 413, p. 127497.

- Jaworski, Z. and Zakrzewska, B., 2002. "MODELLING OF THE TURBULENT WALL JET GENERATED BY A PITCHED BLADE TURBINE IMPELLER: The Effect of Turbulence Model". *Transactions of the Institution of Chemical Engineers*, Vol. 80, p. 846-854.
- Lane, G.L., 2017. "Improving the accuracy of CFD predictions of turbulence in a tank stirred by a hydrofoil impeller". *Chemical engineering science*, Vol. 169, p. 188-211.
- Linek, V., Kordač, M., Fugasová, M., Moucha, T., 2004. Gas-liquid mass transfer coefficient in stirred tanks interpreted through models of idealized eddy structure of turbulence in the bubble vicinity. *Chemical Engineering and Processing*, Vol. 43, p. 1511-1517.
- Menter, R.F., 2009. "Review of the shear-stress transport turbulence model experience from an industrial perspective". *International Journal of Computational Fluid Dynamics*, Vol. 23, No. 4, p. 205-316.
- Murthy, B.N. and Joshi, J.B., 2008. "Assessment of standard k-, RSM and LES turbulence models in a baffled stirred vessel agitated by various impeller designs". *Chemical Engineering Science*, Vol. 63, p. 5468-5495.
- Paul, E. L., Atiemo-Obeng, V. A., Kresta, S. M., 2004. *Handbook of Industrial Mixing: Science and Practice*. John Wiley & Sons.
- Roache, P. J, 1994. Perspective: "A Method for Uniform Reporting of Grid Refinement Studies". *Journal of Fluids Engineering*, Vol. 116, p. 405-413.
- Singh, H., Fletcher, D.F. and Nijdam, J.J., 2011. "An assessment of different turbulence models for predicting flow in a baffled tank stirred with a Rushton turbine". *Chemical Engineering Science*, Vol. 66, p. 5976-5988.
- Wodołazski, A., 2019. "Co-simulation of CFD-multiphase population balance coupled model aeration of sludge flocs in stirrer tank bioreactor". *International Journal of Multiphase Flow*, Vol. 123, p. 103162.
- Yeoh, S.L., Papadakis, G. and Yianneskis, M., 2004. "NUMERICAL SIMULATION OF TURBULENT FLOW CHARACTERISTICS IN A STIRRED VESSEL USING THE LES AND RANS APPROACHES WITH THE SLIDING/DEFORMING MESH METHODOLOGY". *Chemical Engineering Research and Design*, Vol. 82, p. 834-848.

7. RESPONSIBILITY NOTICE

The authors are the only responsible for the printed material included in this paper.